Version of Record: https://www.sciencedirect.com/science/article/pii/S0967066121002367
Manuscript_29318d91a46d0c4870b0eeb3dbc740ac

Degradation Identification and Prognostics of Proton Exchange Membrane Fuel Cell Under Dynamic Load

Meiling Yue[a,1], Zhongliang Li[b], Robin Roche[c], Samir Jemei[a], Noureddine Zerhouni[d]

[a] *FEMTO-ST Institute, FCLAB, Univ. Bourgogne Franche-Comté, CNRS, Belfort, France*
[b] *LIS Laboratory, Aix-Marseille University, CNRS, Marseille, France*
[c] *FEMTO-ST Institute, FCLAB, Univ. Bourgogne Franche-Comté, UTBM, CNRS, Belfort, France*
[d] *FEMTO-ST Institute, FCLAB, Univ. Bourgogne Franche-Comté, ENSMM, CNRS, Belfort, France*

Abstract

Proton exchange membrane (PEM) fuel cell has seen its recent increasing deployment in both automotive and stationary applications. However, the unsatisfied durability of the fuel cell has barriered in the way of its successful commercialization. Recent research on prognostics and predictive maintenance has demonstrated its effectiveness in predicting the system failure and improving the durability of the PEM fuel cell. This paper contributes to developing a degradation identification method for the PEM fuel cell operating under dynamic load. A degradation indicator is proposed based on the polarization model and the nonlinear regression method is applied to extract the degradation feature by segmenting the voltage measurement. To perform prognostics, a machine learning method based on a multi-step echo state network is developed, in which a sliding window is used to recursively reformulate the input sequence with predicted values in the prediction phase. The length of the sliding window is optimized by a genetic algorithm. The proposed method is verified on the experimental PEM fuel cell degradation data and improves the prediction performance on both accuracy and computation speed when comparing with other prognostics methods.

Keywords:
dynamic load, echo state network, PEM fuel cell, health indicator, prognostics

1. Introduction

Although fossil fuels still account for the majority of global energy demand, an energy transition is taking place. Hydrogen, as one of the cleanest fuels, has driven increasing attention around the world, which is regarded as a potential solution to today's environmental problems and resource exhaustion. Using hydrogen as the fuel, ~~To make use of hydrogen, fuel cell re-electrification is a preferable way to maximize its potential benefits, as~~ fuel cells can convert the chemical energy of the hydrogen into electrical energy directly with an efficiency up to 60 to 80%, while the by-product is only water. Among different types of fuel cells, proton exchange membrane (PEM) fuel cells, which take advantages of their fast start-up characteristics and low operating temperatures, are now commercially applied in a variety of stationary and embedded applications [1].

On the road to the massive commercialization of PEM fuel cells, enhancing their durability is a prior challenge. The currently achieved durability of PEM fuel cells in automotive applications is around 4000 - 5000 hours, while an 8000-hour lifetime is the ultimate goal [2]. Efforts have been made to investigate PEM fuel cell degradation mechanisms, especially for those operating under dynamic load [3, 4]. For example, dynamic vehicle cycles in rated and idling conditions are simulated in [5], in which the PEM fuel cell is subjected to different degradation mechanisms causing varying stack voltage degradation rate. An accelerated degradation test is conducted in [6] with normal vehicle driving cycles where signification degradation of the fuel cell has been observed. Varying thermal/humidity state, changing reactant demand and ~~potential~~ voltage cycling are identified as the principal reasons for PEM fuel cell degradation in dynamic operating conditions [7].

Fuel cell performance loss can be easily observed by evaluating the stack voltage degradation and under constant operating conditions, it is measured directly. Various works on PEM fuel cell degradation estimation and prognostics have been conducted using the stack voltage as the direct health indicator [8, 9]. For example, Bressel et al. have proposed to estimate the health state of the PEM fuel cell using an observer-based prognostics algorithm and a state variable was created to track its degradation [10]. Wu et al. have predicted the stack voltage degradation of PEM fuel cells by developing a self-adaptive relevance vector machine, which is able to provide 20 hours ahead forecast time [11]. Both model-based and data-driven prognostics methods have been developed. For example, Pan et al. have proposed a model-based prognostics method based on Electrochemical Impedance Spectroscopy (EIS) measurement and an analytical equivalent circuit model, in which the parameters are obtained by linear regression [12]. A semi-empirical model-based prognostics method based on the adaptive unscented Kalman filter (AUKF) algorithm has been proposed in [13] to improve the initial parameters setting problem. Recent researches have seen increasing interests in developing

[1] Corresponding author. E-mail address: meiling.yue@femto-st.fr

© 2021 published by Elsevier. This manuscript is made available under the CC BY NC user license
https://creativecommons.org/licenses/by-nc/4.0/

data-driven prognostics methods, which can reflect the inherent relationships between the input and output by simulating neural networks and avoid the study of complicated physical mechanisms. Data-driven methods have gradually become the main methodology for fuel cell prognostics due to their easy-to-use and flexible modelling properties [14, 15, 16, 17]. For example, echo state network (ESN) has been deployed to fuel cell prognostics in recent works thanks to its improve computation efficiency [18, 19, 20]. It was first applied to the prediction of the mean cell voltage of a degrading fuel cell in [21] where the accuracy and the computation time are studied regarding the ESN parameters. Furthermore, for predicting the fuel cell health state, a multi-reservoir ESN has been developed in [22] to optimize the parameterization process and in [23], an advanced structure of using moving weight matrix has been proposed to improve the prediction accuracy. However, these studies are limited to the stack level and have not fully considered variable and dynamic loads that may exist in most automotive applications. In those cases, the degradation of the PEM fuel cells cannot be easily quantified using the measured stack voltage, whose value is also affected by system operating dynamics [24]. A degradation indicator reflecting intrinsic degradation level in dynamic operating conditions is required. Some researchers have proposed hybrid degradation indexes in multi-time scales for online operation, however, they are limited to certain components and the accuracy is not satisfying [25]. Li et al. have proposed to represent the dynamic voltage response of the PEM fuel cell using linear parameter-varying models, and then obtained a real-time health indicator based on the online identified model [18]. However, the proposed health index in [18] only evaluates the overall performance loss and lacks the insights of fuel cell intrinsic degradation analysis. As the degradation of the fuel cell is related not only to the ageing phenomenon but also to the time-varying online operating conditions, developing a degradation identification method adapted to random external conditions is required.

This paper contributes to proposing an innovative degradation identification method for the PEM fuel cell operating in real time, especially under dynamic load. A degradation indicator is proposed based on the fuel cell polarization model, which is extracted using a non-linear regression process regardless of the operation conditions. Following that, a multi-step window-sliding ESN prognostics method is applied to predict the future evolution of the degradation indicator which is identified online. The parameterization of the ESN is optimized by a genetic algorithm that ensures improved prediction performance. The proposed degradation identification and prognostics methods are verified with a long-term operation experimental dataset of PEM fuel cell. ~~As there is no additional device to integrate into the embedded fuel cell system, the prognostics can thus be performed in real time.~~ As the measurements are obtained non-intrusively and the proposed method directly uses the output voltage signal, the prognostics can thus be performed in real time.

The main contributions of this paper can be summarized as follows:

1. A real-time degradation indicator of PEM fuel cells is proposed that can be extracted in both static and dynamic/random operation conditions;
2. An enhanced multi-step ESN-based prognostics strategy is adapted for the prediction purpose;
3. The configuration of the proposed prognostics strategy is optimized through a genetic optimization algorithm;
4. The proposed prognostics strategy is validated by the long-term experimental PEM fuel cell degradation data.

The rest of the paper is organized as follows: Section 2 describes the long-term fuel cell degradation experiment and the dataset used to validate the proposed method. Section 3 explains the degradation identification method and Section 4 presents the enhanced multi-step window-sliding ESN prognostics strategy. Finally, Section 5 concludes the paper.

2. Data description

A long-term fuel cell degradation experiment was carried out in FCLAB Research Federation[2], France, and supported by the PRODIG project, which received funding from region Aquitaine, France. The test bench consists of a hydrogen tank, a pressure reducer, purge valves and hydrogen inlet valves, DC electric loads, DC power modules, two fuel cell stack modules, a compact data acquisition system and a computer for control and data logging. The structure of the two-fuel-cell-stack-module is shown in Figure 1. One of the stack modules is used for the dynamic load test, which is supposed to be applied in electric bicycles and is, therefore, tested using a dynamic load profile acquired in real operating conditions. The fuel cell stack is designed with an open cathode and dead-end anode structure and a 24 Vdc air fan is integrated with the stack for air supply and temperature regulation. The speed of the air fan is regulated by varying the duty cycle of an input PWM signal of 25 kHz so that the temperature is controlled at the optimal level. Moreover, in the cathode side, the air is supplied with an air fan. With the air fan, sufficient quantity of air is guaranteed in normal operation. In other words, the fuel cells always work in the high stoichiometry mode. The pressure in the cathode side is kept equal to the atmosphere pressure. On the anode side, the pressure of hydrogen is fixed, and a purge is performed every 30 seconds. The fuel cells are self-humidified. Some critical parameters of the studied fuel cell stack module are listed in Table 1.

The dynamic load profile is obtained in real operating conditions of a hydrogen bike, which is supplied by a 36 V battery, while the fuel cell is used as a range extender, connected in parallel with the battery. Both are used to supply the bike with an average power demand of 53.6 W. A 2.5-hour operation profile is shown in Figure 2, in which the fuel cell starts up to charge the battery until the battery's state-of-charge (SOC) gets to a pre-defined threshold and shuts down when the battery is fully charged. Based on this profile, the current load profile for the

[2]FCLAB Research Federation: `http://www.fclab.fr/`

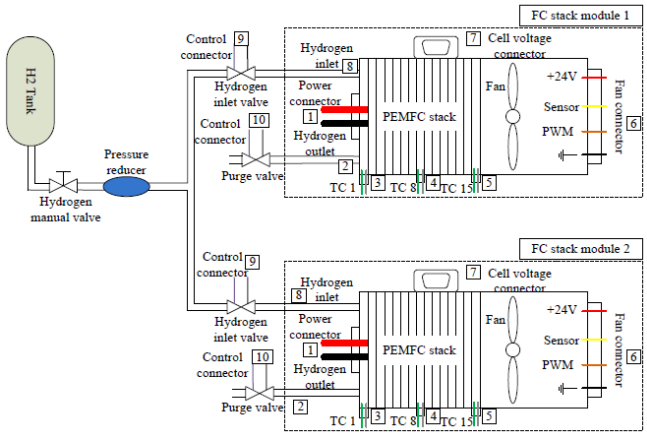

Figure 1: Two-fuel-cell-module structure

Table 1: Parameters of the studied fuel cell stack module

Parameter	Value
Active surface	33.625 cm^2
Number of cells	15
Nominal pressure at hydrogen inlet	0.35 bar
Nominal output power	73.5 W
Maximum operating temperature	75 °C
Maximum current	13.45 A (0.4 A/cm^2)
Lowest permitted stack voltage	7.5 V
Pressure interval at hydrogen inlet	0.1 to 0.4 bar

long-term PEM fuel cell degradation experiment is reproduced to reach 1500 hours of operation time. The stack voltage and the current are recorded with a sampling frequency of 5 Hz and the characterization of the stack is performed every week by collecting polarization curves.

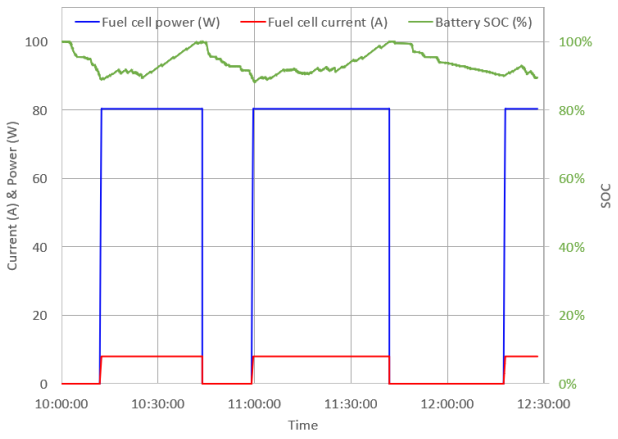

Figure 2: Test profile of a hydrogen bike

The measured stack voltage is shown in Figure 3. Some details of the stack voltage and the corresponding current profile are plotted in Figure 4 (a) and Figure 4 (b), respectively. Some unintentional stops happen during the experiment due to test bench incidents. As the degradation of the fuel cell is on a longer time scale, i.e., thousands of hours, the stops have little influence on its long-term performance loss.

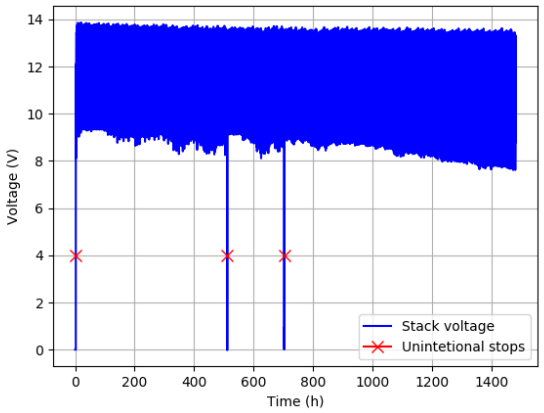

Figure 3: Stack voltage evolution in the dynamic operating test

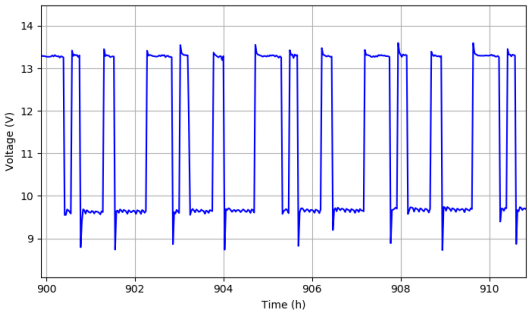

(a) Details of the stack voltage evolution

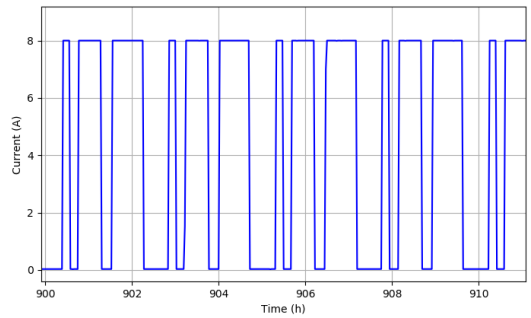

(b) Details of the current profile

Figure 4: Details of the stack voltage and the corresponding current profile

3. Degradation Identification

The performance loss process of the PEM fuel cell stack shown in Figure 3 may be due to different causes, e.g., varying thermal and humidity state, fuel starvation, cycling with large voltage dynamics, etc. It is hard to represent its performance loss by the stack voltage evolution as it is also dependent on the load characteristics and system dynamics. Confronted with this problem, a ~~time-varying~~ degradation indicator is proposed

in this section to evaluate the degradation of the PEM fuel cell operating under such dynamic load.

3.1. Fuel cell polarization model

The polarization test is a common method to characterize a fuel cell. Polarization curve displays the stack voltage output V_{fc} against its operating current i. The polarization curve model of a n-cell fuel cell can be built as the reversible cell voltage V_0 subtracting several irreversible losses including the activation losses and the crossover losses $V_{act+cross}$, the ohmic losses V_{ohmic}, the concentration losses V_{conc}:

$$V_{fc} = nV_{cell} = n(V_0 - V_{act+cross} - V_{ohmic} - V_{conc}) \quad (1)$$

A detailed parametric model of V_{cell} is derived in [26, 27]:

$$V_{cell}(i) = V_0 - \frac{RT}{2aF}\ln\left(\frac{i_{loss}+i}{i_0}\right) - iR_{eq} - B_c\ln\left(1-\frac{i}{i_L}\right) \quad (2)$$

where R is the gas constant, T is the operating temperature, F is the Faraday constant, a is charge transfer coefficients of the electrodes, i_{loss} is the stack internal current, which is assumed to be assimilated to the hydrogen crossover current alone and there is no current caused by membrane shorting, i_0 is the exchange current at the electrodes, R_{eq} is the equivalent ohmic resistance, B_c is an empirical parameter considering the water and gas accumulation effects and i_L is the limiting current at the cathode [27].

3.2. Degradation description

To find an adequate degradation indicator for the PEM fuel cell operating under dynamic current, it is important to know that which component degradation will cause which parameter varies in (2). Some parameters, like R and F, are constant. T is controlled in the experiment so that it is also regarded as constant, so as V_0. Some parameters are difficult to know whether they vary with time or not, therefore, they are set to fit the model with the measurements, namely a and B_c. i_{loss} is not considered as it is assumed to be assimilated to the hydrogen crossover current. Thus, the variations of the left three parameters, R_{eq}, i_0 and i_L, should be considered as the source of degradation.

R_{eq}: The resistance increase can be caused by various phenomena. It includes the electronic and contact resistance increase, as well as the ionic resistance increase related to the membrane degradation [27]. The increase of the electronic and contact resistance can be observed at the surface layer of the bipolar plates, the electrode/electrolyte interface, etc, while the increase of the ionic resistance is dominant by the electrolyte materials and influenced by the membrane water concentration and temperature [28].

i_0: The effective exchange current is a function of the electrode catalyst loading and the catalyst specific surface area [29]. For the fuel cell operated under dynamic load, the cycling will lead to the major degradation of the electrodes: the catalyst layer degradation and the carbon support degradation, especially, the catalyst loss is aggravated by the potential cycles [30].

i_L: The limiting current on the cathode varies due to the changes on the diffusivity of oxygen, the gas pressure and the thickness of the gas diffusion layer [31]. The diffusivity and the pressure of the oxygen at the cathode are dominated cause of the concentration loss, which are influenced by the gas and water accumulation and can be recovered or mitigated by proper water management. The thickness of the gas diffusion layer cannot change over some nanometers, therefore, it can be ignored [27].

Some works have modelled the variation of the three parameters using physical models or semi-empirical models, however, some of them are developed with assumptions, which have not been validated [27]. Moreover, complex parameters bring difficulties when performing prognostics and some measurements needed in the model are not economically or technically feasible, therefore, establishing a degradation indicator that can track the degradation of the PEM fuel cell is necessary.

3.3. Degradation indicator α

Figure 5 plots the polarization curves measured in the 2nd, 4th, 5th, 8th and 9th weeks, which indicates different degrees of fuel cell degradation. The polarization curves were obtained by varying the current value between 0 and the maximum (10 A). 8 current values, as shown in Figure 5, were set increasingly to the test stack through an electronic load. For each test point, the current value was maintained for 10 minutes to get a stable voltage measurement. Then the polarization curves were formed by interconnecting the 8 test points in current-voltage coordinate plane.

The model of (2) is identified with different values of R_{eq}, i_0 and i_L, whereas the evolutions of the parameters are shown in Figure 6. From Figure 6, it is found that the equivalent resistance R_{eq} increases by approximately 80%, while the exchange current i_0 decreases by a rather same value. The fitting result of i_L has remained nearly constant. It is due to that under the dynamic cycling load, the water accumulation is well managed and contributes rarely to the concentration loss. This observation inspires us to assume the same linear evolution of R_{eq} and i_0 and assign a constant value to i_L. Therefore, a unique time-varying variable $\alpha(t)$ is chosen to describe the deviation of the parameters, which reflects the state of health of the fuel cell:

$$R_{eq} = R_{eq,init} \cdot (1 + \alpha(t)) \quad (3)$$

$$i_0 = i_{0,init} \cdot (1 - \alpha(t)) \quad (4)$$

The introduction of variable $\alpha(t)$ ensures the identification of the fuel cell degradation level in the dynamic operation of the fuel cell. Even if the stack is operated under random load and the degradation cannot be directly identified by the voltage signal, $\alpha(t)$ can be used as a degradation indicator to ~~predict~~ indicate the health state of the fuel cell.

As degradation can only be observed over long periods of at least several hundred hours, the fuel cell degradation is supposed to be quasi-constant on a short time scale, i.e., several hours [10, 32]. It allows us to segment the operation time into

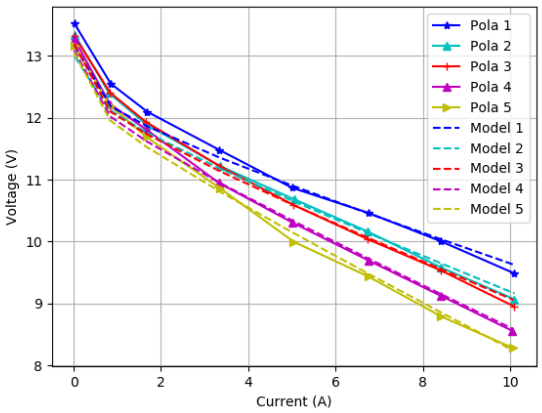

Figure 5: Polarization curves fitted with different α values

short periods and fits the model with different α values on each segment. This is realised by wrapping the pre-defined function as a model, which contains several parameters and an independent variable α, and fitting it using the Levenberg-Marquardt algorithm [33]. The pseudo-code is shown in Algorithm 1.

Algorithm 1 Identification of the degradation indicator α

```
Load available measurement data of I, V          ▷ Load data
Initialize the parameters in model (2)           ▷ Initialization
Define:
Interval = l
Number of steps = j
Time step i = 0
for i = 0, ..., j, do
    Define model (2) with (3) and (4)            ▷ Model definition
    Input X = I[0 + i * l : l + i * l]           ▷ Segmentation
    Output Y = V[0 + i * l : l + i * l]
    Fit the model with α and find the best fit   ▷ Model fit
end for
```

The identification result is shown in Figure 7 and the details are in Figure 8, in which the voltage measurement is segmented with an interval of 3 hours. It can be noticed that the voltage dynamics in load transition periods are not well established using the identified degradation indicator and the polarization curve model. In fact, the voltage dynamics in transition states are mainly caused by system dynamics, such as thermal dynamics, which is not considered in the polarization curve model. The evolution of the extracted α is shown in Figure 9, in which some recoveries in the signal are observed. These recoveries are reversible degradation phenomena due to the characterizations, which are of different operating conditions that affect the gas and water diffusion within the cells are affected. However, these reversible phenomena are part of transient regimes and will disappear once the stack comes back to a permanent regime. As the implementation of prognostics relies on the degradation information contained in the signal, the extracted α is smoothed using a Savitzky–Golay filter to avoid the influence of disturbing information.

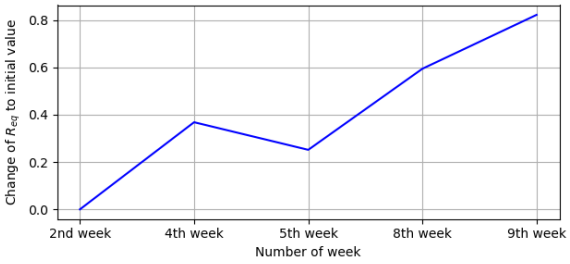

(a) Change of R_{eq} to its initial value

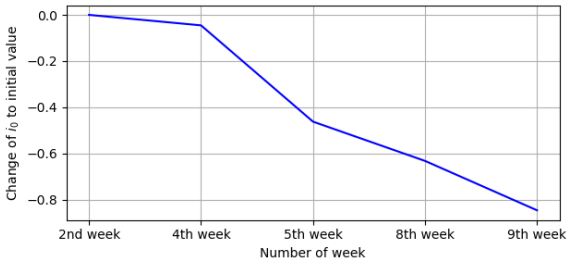

(b) Change of i_0 to its initial value

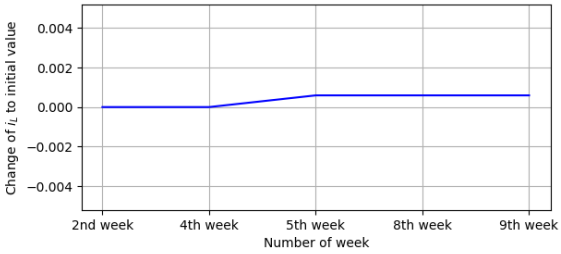

(c) Change of i_L to its initial value

Figure 6: Evolution of degradation parameters R_{eq}, i_0 and i_L

4. ESN-based prognostics method

A data-driven prognostics method based on neural network modelling is proposed in this section. The idea is to use the available dataset to build the system behaviour model and to project the current system state to the future. Data-driven prognostics methods have the model-free advantage that can be applied regardless of the physical characteristics of the system. In this section, a typical recurrent neural network (RNN), i.e., the ESN, is adapted for the prognostics purpose.

4.1. Principle of ESN

The ESN has seen its wide use in time-series prediction applications [34]. Different from traditional RNNs, the ESN uses a "reservoir pool" to build the structure of nonlinear systems, which achieves high prediction speed and competitive prediction performance. The implementation of the ESN is shown in Figure 10 and explained in what follows.

The state update model of ESN is written as:

$$\tilde{\mathbf{u}}(t) = f(\mathbf{w}_{res}\mathbf{u}(t-1) + \mathbf{w}_{in}\mathbf{x}(t)) \quad (5)$$

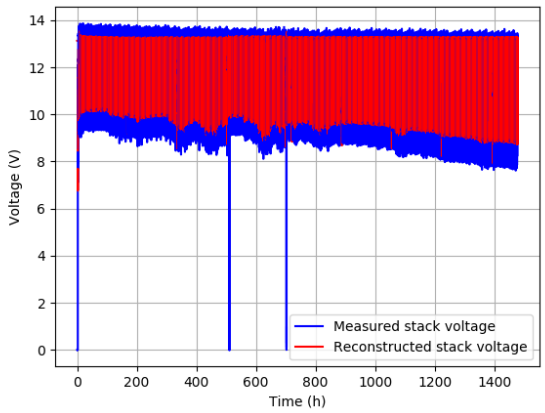

Figure 7: Reconstructed and measured stack voltages

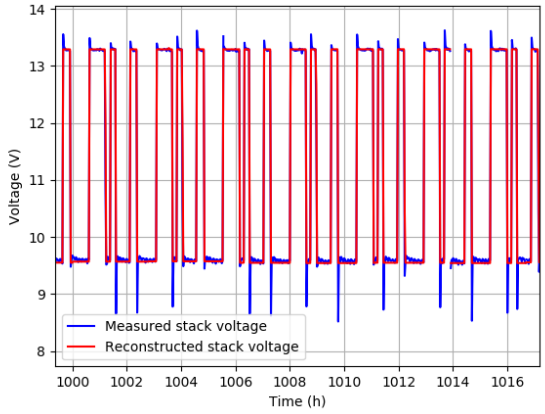

Figure 8: Details of the reconstructed and the measured stack voltages

$$\mathbf{u}(t) = (1-k)\mathbf{u}(t-1) + k\tilde{\mathbf{u}}(t) \tag{6}$$

$$\mathbf{y}(t) = g(\mathbf{w}_{out}\mathbf{u}(t)) \tag{7}$$

where $\mathbf{x}(t) \in \mathbb{R}^{N_x}$ and $\mathbf{y}(t) \in \mathbb{R}^{N_y}$ are the input and output, which, in this study, are the sequences of the degradation indicator α, $\mathbf{u}(t) \in \mathbb{R}^{N_u}$ is the internal state in the reservoir and $\tilde{\mathbf{u}}(t) \in \mathbb{R}^{N_u}$ is its update, $\tilde{\mathbf{u}}(t) = \mathbf{u}(t) - \mathbf{u}(t-1)$, $\mathbf{w}_{in} \in \mathbb{R}^{N_u \times (1+N_x)}$ is the input weight matrix, $\mathbf{w}_{res} \in \mathbb{R}^{N_u \times N_u}$ is the recurrent weight matrix in the reservoir, and $\mathbf{w}_{out} \in \mathbb{R}^{N_y \times (1+N_x+N_u)}$ is the output weight matrix. k is the leaking rate with a range of $(0, 1]$. The *tanh* function is generally adopted as the activation function $f(\bullet)$ of the reservoir, and $g(\bullet)$ of the output layer could be defined with a simple linear function such as $g(\bullet) = 1$. $\mathbf{w}_{in}$ and $\mathbf{w}_{res}$ are initialized randomly and they are constant so that there is no need to train them. Only $\mathbf{w}_{out}$ is going to be trained by linear regression. When the training dataset is provided, denoted as $\mathbf{X}_t = [\mathbf{x}(1), ..., \mathbf{x}(N_t)]$ and $\mathbf{Y}_t = [\mathbf{y}(1), ..., \mathbf{y}(N_t)]$, where N_t is the number of sequences in the input and the output, the corresponding reservoir states, $\mathbf{U}_t = [\mathbf{u}(1), ..., \mathbf{u}(N_t)]$ can be calculated according to (5) and (6). The output weight matrix is calculated as:

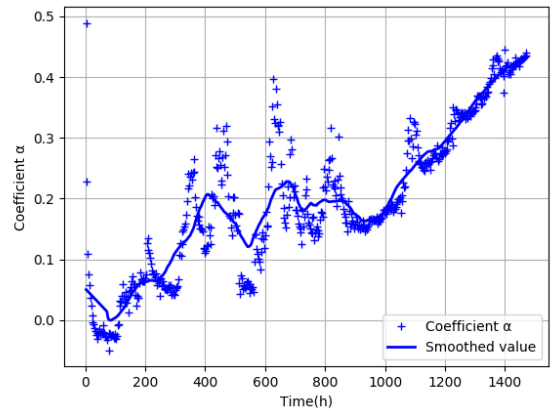

Figure 9: Evolution of the dynamic degradation indicator α

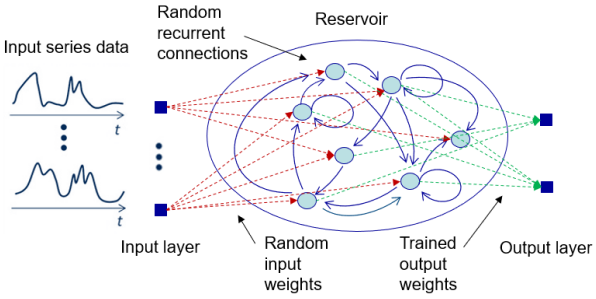

Figure 10: ESN structure illustration

$$\mathbf{w}_{out} = (\Psi_t^T \Psi_t + \lambda \mathbf{I})^{-1} \Psi_t^T \mathbf{Y}_t \tag{8}$$

where $\mathbf{I}$ is N_u order unit matrix, λ is the regulation parameter and

$$\Psi = [1; \mathbf{X}_t; \mathbf{U}_t] = \begin{bmatrix} 1 & 1 & \dots & 1 \\ \mathbf{x}(1) & \mathbf{x}(2) & \dots & \mathbf{x}(N_t) \\ \mathbf{u}(1) & \mathbf{u}(2) & \dots & \mathbf{u}(N_t) \end{bmatrix} \tag{9}$$

The general working procedure is as following:

1. Choose the size of the reservoir N_u and other parameters concerning the level of sparsity of connection, as well as the leakage;
2. Generate the input weights $\mathbf{w}_{in}$ by sampling from a random binomial distribution;
3. Generate the reservoir weights $\mathbf{w}_{res}$ by sampling from a uniform distribution;
4. Calculate the update of the state in the reservoir as the activation function $f(\bullet)$ of the input at the current time step multiplied by the weights plus the previous state multiplied by the the reservoir weights, as written in (5);
5. Create input sequences and connect them to the desired outputs using linear regression and obtain the trained ESN.

Based on the procedure of training an ESN, an input window and a prediction window need to be defined, which are used to formulate the input sequences and the output sequences of the ESN, respectively. The input window length is the length of the input sequence and the prediction window length is how many steps are going to be predicted following the input sequence. The input window length and the prediction window length are selected according to the volume of available input data. Supposing the number of available measurements s is up to N, a window length of p is used for the input sequence, written as:

$$\mathbf{x}(i) = [s(i+1), s(i+2), ..., s(i+p)],\ i = 0, ..., N-p \quad (10)$$

For simplicity, it is written $\mathbf{x}(i) = [s(i+1) : s(i+p)]$ in the following text. Then, the corresponding output with a prediction window length of q is written as:

$$\mathbf{y}(i) = [\hat{s}(i+p+1), \hat{s}(i+p+2), ..., \hat{s}(i+p+q)],\quad i = 0, ..., N-p \quad (11)$$

Similarly, it is written with the form of $\mathbf{y}(i) = [\hat{s}(i+p+1) : \hat{s}(i+p+q)]$ in the following text.

4.2. Adapt ESN for prognostics purpose

The prognostics process can be summarized as a process of estimating a system's remaining useful life and the uncertainties. The international organization for standardization (ISO) committee has defined prognostics as [35]:

> Standard ISO 13381 (2004). *The aim of prognostics is the "estimation of time to failure and risk for one or more existing and future failure modes".*

Therefore, to perform prognostics, we need to predict the system performance until the system failure. Based on the time series forecasting process described in Section 4.1, the last p-length sequence in the training phase is used to predict a sequence with the length of q. Then, the prognostics starts, in which we cannot predict the subsequent states because the input sequences run out, the prediction cannot continue. As we need to continue to predict the time series until the end of life of the system, new input sequences should be formulated to successively move the input window. Thus, to retain the degradation tendency and to manage the prediction uncertainty, the predicted values of the last step with a sliding window of length m are reinjected to the input sequence of the next step, as shown in Figure 11. Therefore, the last m values of the input sequence are indeed the predicted values. This process allows the continuous formulation of the input even without measurements so that the prognostics can be realised. This process is repeated until reaching the end-of-life (EOL) threshold, which, in this paper, is supposed to be the value of 0.423, 97% of the maximum degradation of the tested fuel cell regarding the length of the experiment. ~~1400 hours for the tested fuel cell.~~

The pseudo-code of implementing ESN adapted for prognostics purpose is shown as Algorithm 2, where N_{train} is the number of training steps equal to $N-p$ and $N_{predict}$ is the prediction steps until the system's EOL.

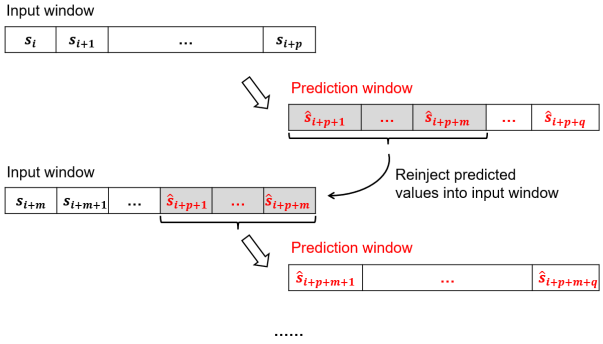

Figure 11: ESN adapted for prognostics purpose

4.3. Implementation of ESN-based prognostics

In order to optimize the configuration of the ESN, the proposed ESN-based prognostics method consists of three phases: training phase, evaluation phase and prediction phase. The length of the identified degradation indicator α, shown in Figure 9, is also divided into three parts for the use of each phase. The ESN is trained in the training phase using the prepared input and output sequences and then, the following 400 hours are regarded as the evaluation phase. During the evaluation phase, the measurement is supposed to be unavailable so that the output sequence is reformulated by the predicted values of the last step. The trained ESN model is used to output the predictions of α and the real values of α is used to evaluate the performance of the prognostics. ~~and determine optimal parameters of the ESN.~~ Here, the result of prognostics is evaluated by calculating the root mean square error (RMSE), written as (12). In order to find the optimal settings of the ESN, an optimization method, i.e., the genetic algorithm (GA), is applied to generate different parameter combinations and run the prognostics algorithm repeatedly until find the optimal settings. ~~optimize the configuration of the ESN.~~ The idea is to code the unknown parameters into binary digits, known as a chromosome, then, calculate the RMSE on the evaluation phase by selecting, crossover and mutating the chromosomes repeatedly until finding the optimal solution [36]. The advantage of GA is its ability to locate the global optimum or near-global optimum solution without exhausting search of the solution space. Besides, the processing time only increased as the square of the project size and not exponentially. Some configured parameters of the proposed ESN-based prognostics method and the adopted GA are listed in Table 2, where the length of the sliding window of m and the number of reservoir neurons N are optimized by the GA. The influence of other ESN parameters in prognostics results is not so critical and the configuration method in [37] has been adopted.

$$RMSE = \sqrt{\frac{\sum_{k=1}^{n}(x_k - \hat{x}_k)^2}{n}} \quad (12)$$

Finally, in the prediction phase, no measurement is available while the ESN has already been optimized and validated by the evaluation phase, therefore, the data of both the training phase and the evaluation phase ~~are used to train the ESN and output the prognostics results on the prediction phase~~ are entered into

Algorithm 2 ESN for prognostics purpose

Load training dataset **s** ▷ Load data
Smooth the training data ▷ Smoothing
Normalize the training data ▷ Normalization
Define:
Input window length = p
Prediction window length = q
Sliding window length = m
Number of training steps = N_{train}
Number of prediction steps = $N_{predict}$
Time step $i = 0$
while $x_i < x_{EOL}$ **do**
  for $i = 0, ..., N_{train}$, **do** ▷ Training phase
    $y_{train}[i, :] = s[i + p + 1 : i + p + q]$ ▷ Prepare input and output
    $x_{train}[i, :] = s[i : i + p]$
  end for
  Fit the ESN with prepared input x_{train} and output y_{train}
  Initialize $x_{predict}[0, :]$ by connecting $x[N_{train} + m : N_{train} + p]$ and $y_{train}[-1, 0 : m]$
  for $i = 0, ..., N_{predict}$, **do** ▷ Start prognostics
    Predict $y_{predict}[i]$ using the fitted ESN and $x_{predict}[i, :]$
    Reformulate $x_{predict}[i, :]$ by connecting $x_{predict}[i - 1, m : p]$ and $y_{predict}[i, 0 : m]$ ▷ Reformulate input
  end for
end while

Table 2: Configuration of ESN-based prognostics method

Parameter	Value
Input window length p	50
Prediction window length q	10
Leaking rate	0.2
Spectral radius	0.6
Regression parameter	0.01
GA population size	100
Number of generations	400
Length of chromosome	10

the trained ESN model and output the prediction results. The whole procedure is shown in Figure 12. The prognostics results are discussed in the following section.

4.4. Result discussion

For comparison, at first, m is fixed at 1. The optimal N is found between 10 and 400 using an iterating loop. The optimal values of N, the RMSEs of the prognostics results in both evaluation and prediction phases and the implementation time with different training data lengths are recorded in Table 3. The prognostics performance on the evaluation phase and the prediction phase, as well as the errors are shown in Figure 13 for a visual check. The beginning of the training phase has lower accuracy because of the insufficient training data. After 200 hours, the training error is closed to zero, which demonstrates that the configure ESN is of good performance. During the evaluation phase, the measurement is supposed to be unavailable so

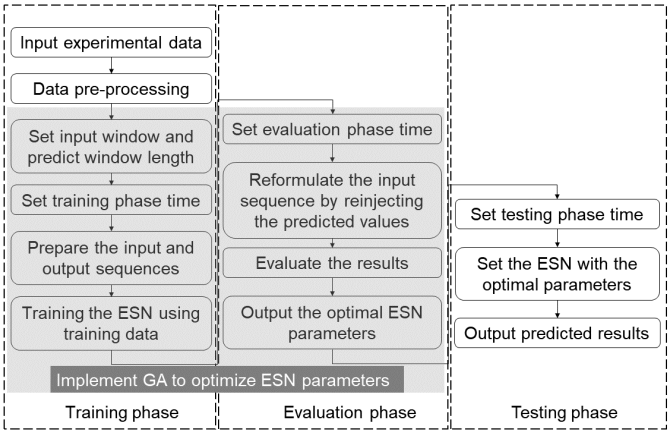

Figure 12: Procedure of ESN-based prognostics method

that the output sequence is reformulated by the predicted values of the last step, as described in Section 4.2. The optimal result is plotted in red dashed line. However, when it comes to the prediction phase, the RMSEs get worse. This is because there is only one predicted value being considered in the next step, which could be accidental and cannot transfer enough information. Moreover, the implementation time of GA is less than 1 minute, while the implementation time of ESN-based prognostics is less than 1 second.

Table 3: ESN-based prognostics results (m=1)

Training data length (hours)	500	600	700	800
m	1	1	1	1
N	90	94	83	81
RMSE of training	0.036	0.019	0.012	0.017
RMSE of evaluation	0.030	0.032	0.056	0.039
RMSE of prediction	0.112	0.140	0.304	0.182
Prognostics implementation time	0.93s	0.94s	0.93s	0.94s

Figure 14 shows the prognostics results with different training data lengths, in which both m and N are optimized. The GA optimization results of the two parameters and the RMSEs of both the evaluation phase and the prediction phase, together with the improvements compared with Table 3 are shown in Table 4. By optimizing the number of values that are reinjected into the input sequence of the next step, prognostics results in the prediction phase have been improved up to 90.8%.

4.5. Comparison with different methods

The proposed prognostics method is compared with different methods in the literature. The comparison methods include particle filter [9] and stacked long short-term memory (LSTM) [38]. The training phase considers the same generated samples. In the compared particle filter method, a second order exponential model is used, and the details of model parameters of particle filter prognostics method is listed in Table 5. The stacked LSTM used for comparison is with two hidden layers

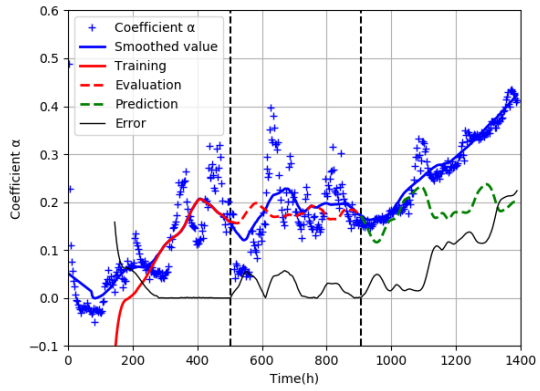

(a) Prediction result with training data length = 500 hours

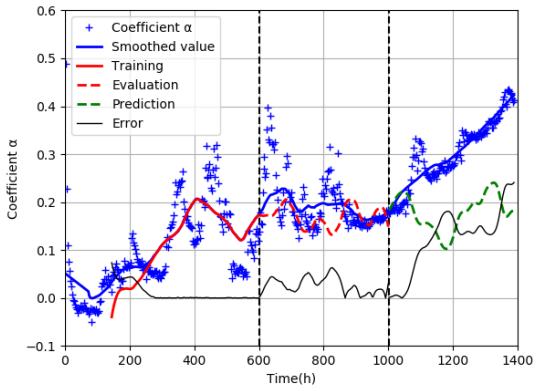

(b) Prediction result with training data length = 600 hours

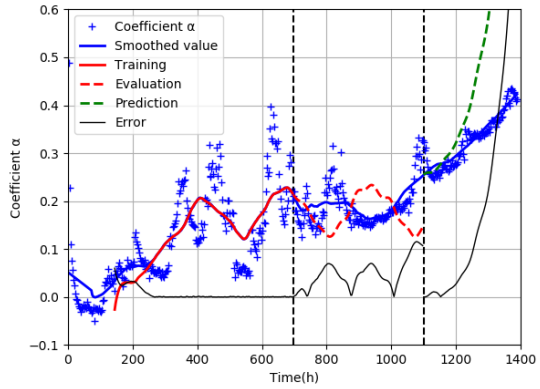

(c) Prediction result with training data length = 700 hours

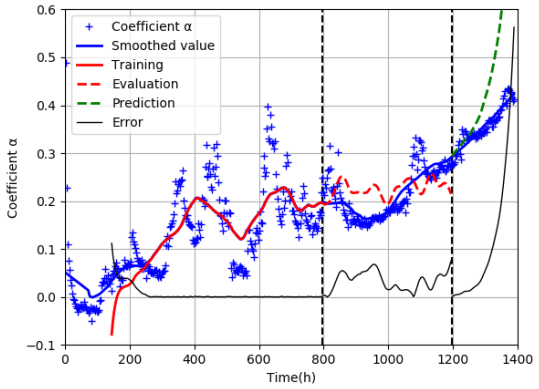

(d) Prediction result with training data length = 800 hours

Figure 13: Implementation of prognostics with different training data lengths (optimizing N)

Table 4: GA optimization and ESN-based prognostics results (optimizing m)

Training data length (hours)	500	600	700	800
Optimized m	3	5	3	3
Optimized N	95	80	234	265
RMSE of training	0.017	0.019	0.019	0.005
RMSE of evaluation	0.031	0.039	0.047	0.033
Improvements of evaluation	-3.3%	2.5%	16.1%	1.5%
RMSE of prediction	0.051	0.017	0.028	0.020
Improvements of prediction	54.5%	87.9%	90.8%	89.0%
Prognostics implementation time	0.91s	0.90s	1.12s	1.03s

Table 5: Model parameters of particle filter prognostics method

Parameter	Value
Input dimension	1
Output dimension	1
Number of state variables	7
Number of particles	2000

and a dense (output) layer for prediction. The details of the configuration of the stacked LSTM prognostics method is shown in Table 6.

The performance of the three different prognostics method is compared in Table 7. As it can be seen from Table 7, the proposed multi-step ESN-based prognostics method has achieved the best prediction accuracy at 600-hour, 700-hour and 800-hour training data length, while the accuracy is worse than the particle filter method at 500-hour training data length. This is because when more information is fed to the model, the model can leverage more trend information, thus improving the prediction accuracy. Besides, the performance of stacked LSTM prognostics method is the worst due to the non-optimized configurations. When comparing the implementation time, the proposed ESN runs the fastest, which is more competitive for online applications.

5. Conclusion

A degradation identification and prognostics method for real-time operating PEM fuel cells was proposed in this paper. The degradation indicator was derived based on the polarization model and could be extracted from the stack voltage measurements with random system dynamics. To perform prognostics, an enhanced multi-step ESN was adapted for the prediction purpose and the parameters of the ESN were optimized through an

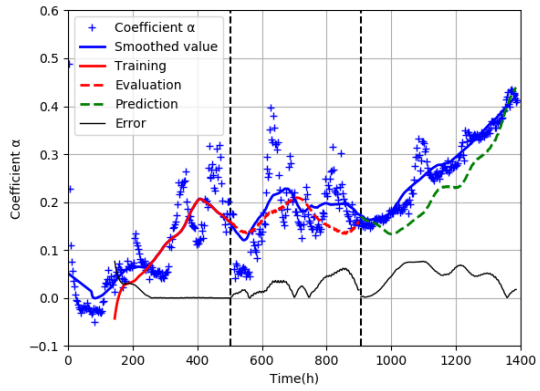

(a) Prediction result with training data length = 500 hours

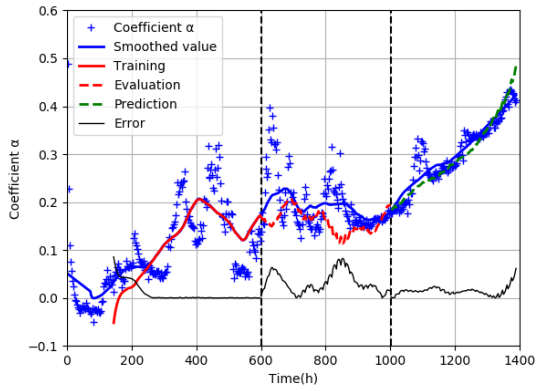

(b) Prediction result with training data length = 600 hours

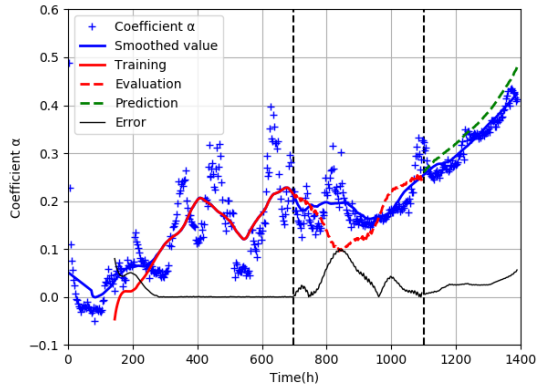

(c) Prediction result with training data length = 700 hours

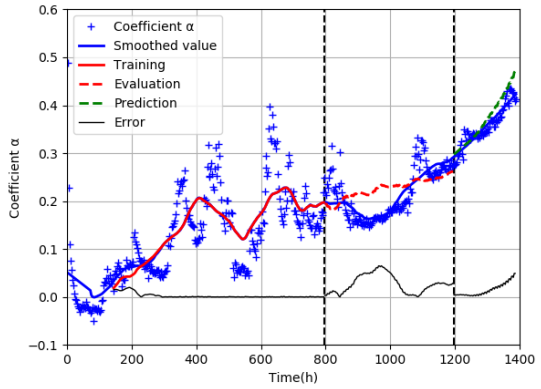

(d) Prediction result with training data length = 800 hours

Figure 14: Implementation of prognostics with different training data lengths (optimizing m and N)

Table 6: Model parameters of stacked LSTM prognostics method

Parameter	Value
Time steps	4
Number of neurons on hidden layer 1	100
Number of neurons on hidden layer 2	100
Number of neurons on dense layer	1
Optimizer	adam
Loss	mean squared error
Epoch number	50
Batch size	50
Dropout rate	0.01

evaluation phase by a genetic algorithm. Compared to non-optimized case, the RMSEs of the predictions were improved up to 90.8% by introducing an optimized sliding window length when reformulating the input of the ESN in the prognostics phase. Moreover, the proposed method achieved better accuracy and less computation time when comparing with other prognostics methods.

The proposed method of degradation identification and prognostics allows one to estimate and predict the PEM fuel cell health state under variable and dynamic operating conditions. The degradation identification can be realized in real time without using supplementary measurements and the prognostics strategy is model-free. This method is control-oriented and can facilitate the development of degradation tolerant control strategies as well as advanced predictive maintenance solutions. The ongoing work is also being conducted to investigate systematically the effect of different factors in dynamic operating conditions, such as the internal water dynamics.

Acknowledgment

This paper is supported by the project HAEOLUS, funded by the Fuel Cells and Hydrogen 2 Joint Undertaking under the European Union's Horizon 2020 research and innovation program under grant agreement No 779469. Any contents herein reflect solely the authors' view. The FCH 2 JU and the European Commission are not responsible for any use that may be made of the information herein contained. This work is also supported by the EIPHI Graduate School (contract ANR-17-EURE-0002) and the project PRODIG (1494C0045) funded by French Environment and Energy Management Agency.

Table 7: Comparison of prognostics methods

Training data length (hour)	500		600		700		800	
	RMSE	Time	RMSE	Time	RMSE	Time	RMSE	Time
Partile filter [9]	0.042	4.19s	0.035	4.45s	0.049	4.73s	0.047	5.25s
Stacked LSTM [38]	0.079	6.81s	0.078	7.31s	0.078	7.11s	0.051	7.47s
Proposed ESN	0.051	0.91s	0.017	0.90s	0.028	1.12s	0.020	1.03s

References

[1] S. Kong, M. Bressel, M. Hilairet, R. Roche, Advanced passivity-based, aging-tolerant control for a fuel cell/super-capacitor hybrid system, Control Engineering Practice 105 (2020) 104636. doi:https://doi.org/10.1016/j.conengprac.2020.104636.

[2] J. M. Kurtz, H. N. Dinh, Fuel cell technology status: Degradation, Tech. rep., National Renewable Energy Lab.(NREL), Golden, CO (United States) (2018).

[3] R. Keller, S. Ding, M. Müller, D. Stolten, Fault-tolerant model predictive control of a direct methanol-fuel cell system with actuator faults, Control Engineering Practice 66 (2017) 99 – 115. doi:https://doi.org/10.1016/j.conengprac.2017.06.008.

[4] J. Luna, E. Usai, A. Husar, M. Serra, Enhancing the efficiency and lifetime of a proton exchange membrane fuel cell using nonlinear model-predictive control with nonlinear observation, IEEE Transactions on Industrial Electronics 64 (8) (2017) 6649–6659. doi:10.1109/TIE.2017.2682787.

[5] G. Wang, F. Huang, Y. Yu, S. Wen, Z. Tu, Degradation behavior of a proton exchange membrane fuel cell stack under dynamic cycles between idling and rated condition, International Journal of Hydrogen Energy 43 (9) (2018) 4471 – 4481. doi:https://doi.org/10.1016/j.ijhydene.2018.01.020.

[6] J. Han, J. Han, S. Yu, Experimental analysis of performance degradation of 3-cell pemfc stack under dynamic load cycle, International Journal of Hydrogen Energy 45 (23) (2020) 13045 – 13054. doi:https://doi.org/10.1016/j.ijhydene.2020.02.215.

[7] P. Ren, P. Pei, Y. Li, Z. Wu, D. Chen, S. Huang, Degradation mechanisms of proton exchange membrane fuel cell under typical automotive operating conditions, Progress in Energy and Combustion Science 80 (2020) 100859. doi:https://doi.org/10.1016/j.pecs.2020.100859.

[8] R. Ma, T. Yang, E. Breaz, Z. Li, P. Briois, F. Gao, Data-driven proton exchange membrane fuel cell degradation predication through deep learning method, Applied Energy 231 (2018) 102 – 115. doi:https://doi.org/10.1016/j.apenergy.2018.09.111.

[9] M. Jouin, R. Gouriveau, D. Hissel, M.-C. Péra, N. Zerhouni, Prognostics of pem fuel cell in a particle filtering framework, International Journal of Hydrogen Energy 39 (1) (2014) 481 – 494. doi:https://doi.org/10.1016/j.ijhydene.2013.10.054.

[10] M. Bressel, M. Hilairet, D. Hissel, B. Ould Bouamama, Remaining useful life prediction and uncertainty quantification of proton exchange membrane fuel cell under variable load, IEEE Transactions on Industrial Electronics 63 (4) (2016) 2569–2577. doi:10.1109/TIE.2016.2519328.

[11] Y. Wu, E. Breaz, F. Gao, D. Paire, A. Miraoui, Nonlinear performance degradation prediction of proton exchange membrane fuel cells using relevance vector machine, IEEE Transactions on Energy Conversion 31 (4) (2016) 1570–1582. doi:10.1109/TEC.2016.2582531.

[12] R. Pan, D. Yang, Y. Wang, Z. Chen, Health degradation assessment of proton exchange membrane fuel cell based on an analytical equivalent circuit model, Energy 207 (2020) 118185. doi:https://doi.org/10.1016/j.energy.2020.118185.

[13] H. Liu, J. Chen, C. Zhu, H. Su, M. Hou, Prognostics of proton exchange membrane fuel cells using a model-based method, IFAC-PapersOnLine 50 (1) (2017) 4757 – 4762, 20th IFAC World Congress. doi:https://doi.org/10.1016/j.ifacol.2017.08.947.

[14] H. Liu, J. Chen, D. Hissel, H. Su, Short-term prognostics of pem fuel cells: A comparative and improvement study, IEEE Transactions on Industrial Electronics 66 (8) (2019) 6077–6086. doi:10.1109/TIE.2018.2873105.

[15] R. Ma, Z. Li, E. Breaz, C. Liu, H. Bai, P. Briois, F. Gao, Data-fusion prognostics of proton exchange membrane fuel cell degradation, IEEE Transactions on Industry Applications 55 (4) (2019) 4321–4331. doi:10.1109/TIA.2019.2911846.

[16] D. Zhou, A. Al-Durra, K. Zhang, A. Ravey, F. Gao, A robust prognostic indicator for renewable energy technologies: A novel error correction grey prediction model, IEEE Transactions on Industrial Electronics 66 (12) (2019) 9312–9325. doi:10.1109/TIE.2019.2893867.

[17] J. Ma, X. Liu, X. Zou, M. Yue, P. Shang, L. Kang, S. Jemei, C. Lu, Y. Ding, N. Zerhouni, Y. Cheng, Degradation prognosis for proton exchange membrane fuel cell based on hybrid transfer learning and intercell differences, ISA Transactions (2020). doi:https://doi.org/10.1016/j.isatra.2020.06.005.

[18] Z. Li, Z. Zheng, R. Outbib, Adaptive prognostic of fuel cells by implementing ensemble echo state networks in time-varying model space, IEEE Transactions on Industrial Electronics 67 (1) (2020) 379–389.

[19] S. Morando, S. Jemei, D. Hissel, R. Gouriveau, N. Zerhouni, Proton exchange membrane fuel cell ageing forecasting algorithm based on echo state network, International Journal of Hydrogen Energy 42 (2) (2017) 1472–1480. doi:https://doi.org/10.1016/j.ijhydene.2016.05.286.

[20] Z. Hua, Z. Zheng, M.-C. Péra, F. Gao, Remaining useful life prediction of pemfc systems based on the multi-input echo state network, Applied Energy 265 (2020) 114791. doi:https://doi.org/10.1016/j.apenergy.2020.114791.

[21] S. Morando, S. Jemei, R. Gouriveau, N. Zerhouni, D. Hissel, Fuel cells prognostics using echo state network, in: IECON 2013 - 39th Annual Conference of the IEEE Industrial Electronics Society, 2013, pp. 1632–1637. doi:10.1109/IECON.2013.6699377.

[22] R. Mezzi, S. Morando, N. Y. Steiner, M. C. Péra, D. Hissel, L. Larger, Multi-reservoir echo state network for proton exchange membrane fuel cell remaining useful life prediction, in: IECON 2018 - 44th Annual Conference of the IEEE Industrial Electronics Society, 2018, pp. 1872–1877. doi:10.1109/IECON.2018.8591345.

[23] Z. Hua, Z. Zheng, M. C. Péra, F. Gao, Data-driven prognostics for pemfc systems by different echo state network prediction structures, in: 2020 IEEE Transportation Electrification Conference Expo (ITEC), 2020, pp. 495–500. doi:10.1109/ITEC48692.2020.9161581.

[24] Z. Li, S. Jemei, R. Gouriveau, D. Hissel, N. Zerhouni, Remaining useful life estimation for pemfc in dynamic operating conditions, in: 2016 IEEE Vehicle Power and Propulsion Conference (VPPC), 2016, pp. 1–6. doi:10.1109/VPPC.2016.7791762.

[25] H. Liu, J. Chen, D. Hissel, J. Lu, M. Hou, Z. Shao, Prognostics methods and degradation indexes of proton exchange membrane fuel cells: A review, Renewable and Sustainable Energy Reviews 123 (2020) 109721. doi:https://doi.org/10.1016/j.rser.2020.109721.

[26] O. Z. Sharaf, M. F. Orhan, An overview of fuel cell technology: Fundamentals and applications, Renewable and Sustainable Energy Reviews 32 (2014) 810–853. doi:https://doi.org/10.1016/j.rser.2014.01.012.

[27] M. Jouin, R. Gouriveau, D. Hissel, M.-C. Marion-Péra, N. Zerhouni, Degradations analysis and aging modeling for health assessment and prognostics of pemfc, Reliability Engineering and System Safety 148 (2016) 78 – 95. doi:https://doi.org/10.1016/j.ress.2015.12.003.

[28] A. Husar, S. Strahl, J. Riera, Experimental characterization methodology for the identification of voltage losses of pemfc: Applied to an open cathode stack, International Journal of Hydrogen Energy 37 (8) (2012) 7309–7315, iII Iberian Symposium on Hydrogen, Fuel Cells and Advanced Batteries, HYCELTEC-2011. doi:https://doi.org/10.1016/j.ijhydene.2011.11.130.

[29] F. Barbir, Chapter five - fuel cell operating conditions, in: F. Barbir (Ed.), PEM Fuel Cells (Second Edition), second edition Edition, Academic Press, Boston, 2013, pp. 119–157. doi:https://doi.org/10.1016/B978-0-12-387710-9.00005-9.

[30] S. S. Khan, H. Shareef, M. Kandidayeni, L. Boulon, A. Amine,

E. H. Abdennebi, Dynamic semiempirical pemfc model for prognostics and fault diagnosis, IEEE Access 9 (2021) 10217–10227. doi:10.1109/ACCESS.2021.3049528.
[31] J. M. Morgan, R. Datta, Understanding the gas diffusion layer in proton exchange membrane fuel cells. i. how its structural characteristics affect diffusion and performance, Journal of Power Sources 251 (2014) 269–278. doi:https://doi.org/10.1016/j.jpowsour.2013.09.090.
[32] M. Jouin, M. Bressel, S. Morando, R. Gouriveau, D. Hissel, M.-C. Péra, N. Zerhouni, S. Jemei, M. Hilairet, B. Ould Bouamama, Estimating the end-of-life of pem fuel cells: Guidelines and metrics, Applied Energy 177 (2016) 87 – 97. doi:https://doi.org/10.1016/j.apenergy.2016.05.076.
[33] J. J. Moré, The levenberg-marquardt algorithm: Implementation and theory, in: G. A. Watson (Ed.), Numerical Analysis, Springer Berlin Heidelberg, Berlin, Heidelberg, 1978, pp. 105–116.
[34] H. Jaeger, The "echo state" approach to analysing and training recurrent neural networks, GMD Report 148, GMD - German National Research Institute for Computer Science (2001).
[35] ISO13381-1, Condition monitoring and diagnostics of machines e prognostics e part1: general guidelines, International Organization for Standardization (2004).
[36] A. Chipperfield, P. Fleming, C. M. Fonseca, Genetic algorithm tools for control systems engineering, Proceedings of Adaptive Computing in Engineering Design and Control 23 (01 1994). doi:10.1016/S1474-6670(17)49015-X.
[37] M. Lukoševičius, A Practical Guide to Applying Echo State Networks, Springer Berlin Heidelberg, Berlin, Heidelberg, 2012, pp. 659–686. doi:10.1007/978-3-642-35289-8-36.
[38] F.-K. Wang, X.-B. Cheng, K.-C. Hsiao, Stacked long short-term memory model for proton exchange membrane fuel cell systems degradation, Journal of Power Sources 448 (2020) 227591. doi:https://doi.org/10.1016/j.jpowsour.2019.227591.